



Analyst

Investigation of the effect of taurine supplementation on muscle taurine content in the mdx mouse model of Duchenne muscular dystrophy using chemically specific synchrotron imaging

Journal:	<i>Analyst</i>
Manuscript ID	AN-ART-04-2020-000642.R1
Article Type:	Paper
Date Submitted by the Author:	08-Jul-2020
Complete List of Authors:	Terrill, Jessica; The University of Western Australia, School of Molecular Sciences Webb, Samuel; Stanford Synchrotron Radiation Lightsource, SLAC National Accelerator Laboratory Arthur, Peter; The University of Western Australia, School of Molecular Sciences Hackett, Mark; Curtin University, School of Molecular and Life Sciences; Curtin University, Curtin Health Innovation Research Institute (CHIRI)

SCHOLARONE™
Manuscripts

1
2
3 **TITLE:** Investigation of the effect of taurine supplementation on muscle taurine content in the
4 mdx mouse model of Duchenne muscular dystrophy using chemically specific synchrotron
5 imaging
6
7

8 **AUTHOR LIST:** Jessica R. Terrill^a, Samuel M. Webb^b, Peter G. Arthur^a, Mark J. Hackett^{c,d}
9

10 **AFFILIATIONS:**
11

12
13 ^a School of Molecular Sciences, the University of Western Australia, Perth, Western
14 Australia, AUS 6009
15

16
17 ^bStanford Synchrotron Radiation Lightsource, SLAC National Accelerator Laboratory, Menlo
18 Park, California, USA 94025
19

20
21 ^cCurtin University, Curtin Institute for Functional Molecules and Interfaces, School of
22 Molecular and Life Sciences, Perth, Western Australia, AUS 6845
23

24
25 ^dCurtin University Curtin Health Innovation Research Institute, Perth, Western Australia,
26 AUS 6102
27

28 **ABSTRACT:** Duchenne muscular dystrophy (DMD) is a lethal genetic muscle wasting
29 disorder, which currently has no cure. Supplementation with the drug taurine has been
30 shown to offer therapeutic benefit in the mdx model for DMD, however the mechanisms by
31 which taurine protects dystrophic muscle is not fully understood. Mdx muscle is deficient in
32 taurine, however it is not known if this deficiency occurs in the extracellular space, in other
33 cells present in the tissue (such as immune cells) or in the myofibre itself. Likewise, the
34 tissue location of taurine enrichment in taurine treated mdx muscle is not known. In this
35 study we applied X-ray absorption near edge spectroscopy (XANES) at the sulfur K-edge in
36 an imaging format to determine taurine distribution in muscle tissue. XANES is the only
37 technique currently capable of imaging taurine directly in muscle tissue, at a spatial
38 resolution approaching myocyte cell size (20 – 50 µm). Using a multi-modal approach of
39 XANES imaging and histology on the same tissue sections, we show that in mdx muscle, it
40 is the myofibres that are deficient in taurine, and taurine supplementation ameliorates this
41 deficiency. Increasing the taurine content of mdx myofibres was associated with a decrease
42 in myofibre damage (as shown by the percentage of intact myofibres) and inflammation.
43 These data will help drive future studies to better elucidate the molecular mechanisms
44 through which taurine protects dystrophic muscle; they also support the continued
45 investigation of taurine as a therapeutic intervention for DMD.
46
47
48
49
50
51
52
53
54
55

56
57 **KEY WORDS:** taurine, XANES, XAS, synchrotron, sulfur, sulfonic acid, muscle, muscular
58 dystrophy, multi-modal
59
60

INTRODUCTION

Duchenne muscular dystrophy (DMD) is a lethal genetic muscle wasting disorder, with an incidence of approximately 1 in 3500 – 6000 boys worldwide.¹ The condition arises from mutations in the dystrophin gene and the downstream consequence is reduced content of functional dystrophin protein in muscle tissue.² Ultimately, the reduction in functional dystrophin results in repeated cycles of myofibre necrosis, increased inflammation and fibrosis, which eventually lead to death through respiratory or cardiac failure.^{1, 3}

Despite elucidation of the underlying genetic mutation that drives DMD, the full cascade of biochemical events that eventuate in muscle wastage are not fully understood, and there is currently no cure. To further understand the biochemistry of DMD pathology and identify targets for therapeutic interventions, many researchers utilise the mdx mouse model, which is phenotypically similar to the human condition.⁴ Whilst the adult mdx mouse has a very mild pathology, the juvenile mdx mouse undergoes an acute onset of severe myofibre necrosis from 3 weeks; after 6 weeks of age dystropathology has stabilised.^{5, 6} We have focused on the role of inflammation and associated oxidative stress in dystropathology, and have investigated various compounds that target this pathway.⁷⁻¹² One such compound is the semi-essential amino acid taurine (2-aminoethanesulfonic acid), which is found in many tissues and is considered important for the function of skeletal muscle, where it modulates ion channel function, membrane stability and calcium homeostasis, as well as having anti-inflammatory and antioxidant properties.¹³⁻¹⁸ We and others have administered taurine to mdx mice, resulting in a prevention of myofibre necrosis, an improvement in both *in vivo* and *ex vivo* muscle strength, increased fatigue resistance and decreased inflammation and oxidative stress.^{8, 9, 11, 19-23}

Interestingly, we show a whole body dysregulation of taurine metabolism in mdx, across various stages of the disease.²⁴ Importantly, taurine content is reduced in mdx muscle during active dystropathology, which may contribute to muscle wasting. Taurine distribution is found in high concentrations fairly ubiquitously in most animals, however its concentration is especially high (mM) in skeletal and heart muscle; its concentration is lower (μ M) in plasma and extracellular fluid.^{15, 25} The concentration of taurine is also particularly high in immune cells (up to 50 mM in leukocytes), where it protects tissue from oxidant injury.²⁶ Excessive immune cell infiltration is a critical component of DMD and mdx pathology, and thus the measurement of muscle taurine content by classical HPLC assay (on homogenised muscle tissue) is a combination of myofibre taurine content, taurine in the extracellular space and immune cell taurine content. Consequently, the exact tissue location of taurine deficiency in mdx muscle is not known, as is the location in muscle that is enriched after exogenous

1
2
3 taurine treatment (i.e. whether taurine treatment increases taurine content of myofibres or
4 the extracellular space, or increases taurine uptake by immune cells). Identification of the
5 regional taurine distribution in muscle tissue has previously been difficult, owing to the highly
6 mobile and diffusible nature of taurine,²⁷ and lack of a direct imaging method.²⁸ Immuno-
7 histochemistry successfully detects a portion of muscle tissue taurine pool, however the
8 extent to which taurine leaches or is redistributed during the fixation and staining process is
9 not known.^{27, 28} Taurine may be detected by ¹H NMR,²⁹ but spatial resolution is often limited
10 to hundreds of microns at best, and therefore *in vivo* or *ex vivo* NMR imaging is not sufficient
11 to determine cellular localisation.³⁰
12
13
14
15
16
17

18 To increase the understanding of the pathological role of taurine depletion in mdx
19 muscle, and to elucidate the mechanisms through which taurine supplementation exerts
20 therapeutic benefit, the ability to visualise taurine distribution within tissues is needed. X-ray
21 absorption near edge spectroscopy (XANES) at the sulfur K-edge has recently emerged as a
22 novel analytical imaging tool,³¹ to semi-quantitatively detect taurine in biological samples.^{28,}
23 ³²⁻³⁴ XANES was initially used to quantify bulk levels of taurine in cultured cells,³⁴ which has
24 now been extended through protocol development,^{28, 32} specifically XANES-imaging, to
25 image taurine distribution at 10 – 20 μm spatial resolution *ex vivo* in tissue sections.³⁵ The
26 method was validated in brain tissue and enabled visualisation of taurine loss from
27 hippocampal cell layers following global brain ischemia.³⁵ In addition to analysis of taurine,
28 the XANES spectrum at the sulfur K-edge can be used to simultaneously determine relative
29 content of multiple sulfur functional groups, such as thiols, thio-ethers, disulfides, and
30 sulfates.^{36, 37} These functional groups are relevant to mdx pathogenesis, as increased
31 disulfides are an indicator of oxidative stress. Therefore, XANES analyses provides an
32 unprecedented capability to investigate taurine distribution in muscle tissue, offering near-
33 cellular spatial resolution (20 μm)* to associate taurine content and distribution with markers
34 of sulfur metabolism and oxidative stress.
35
36
37
38
39
40
41
42
43
44

45 In this study we have used XANES imaging in combination with Haematoxylin and
46 Eosin (H&E) staining histology on the same tissue sections, to investigate muscle taurine
47 distribution in wildtype mice, mdx mice, and mdx mice treated with taurine. The combination
48 of XANES imaging with histology on the same tissue section has enabled this study for the
49 first time to associate taurine content with necrotic muscle tissue, and with infiltrating
50 immune cells. The results provide direct evidence that although infiltrating immune cells
51 elevate muscle taurine content, taurine treatment gives rise to increased myofibre taurine
52 that is independent of taurine localised within immune cells.
53
54
55
56
57
58
59
60

EXPERIMENTAL

Reagents were purchased from Merck unless specified.

Animal treatment and sampling

Experiments were carried out on dystrophic mdx (C57Bl/10ScSn-*Dmd*^{mdx}) and non-dystrophic control C57 (C57Bl/10ScSn) mice (the parental strain for mdx). All animal experiments were conducted in strict accordance with the guidelines of the National Health and Medical Research Council Code of practice for the care and use of animals for scientific purposes (2004), and the Animal Welfare Act of Western Australia (2002), and were approved by the Animal Ethics committee at the University of Western Australia. All mice were obtained from the Animal Resource Centre, Murdoch, Western Australia. Mice were maintained at the University of Western Australia on a 12-h light/dark cycle, under standard conditions, with free access to food and drinking water. Equal numbers of male and female mice were used for analysis. Mice were weaned at 21 days, and were given either no treatment or 4% (w/v) taurine in the drinking water. Water ingestion and body weights were monitored twice weekly for all mdx treatment groups. No significant differences were observed in the amount of water ingested for any group (data not shown). The approximate consumption of taurine, based on water consumption measured in metabolic cages, was about 10 g/kg/day.

All mice were sampled at 42 days of age (6 weeks). All mice were sacrificed at 6 weeks by cervical dislocation while under terminal anesthesia (2%v/v Attane isoflurane Bomac Australia). Whole blood was collected via cardiac puncture followed by centrifugation, plasma removal, and freezing at -80 °C until analysis. Gastrocnemius and quadriceps muscles (two highly affected muscles) were collected and either snap frozen in liquid nitrogen for neutrophil content or cut in half and mounted on cork board using tragacanth gum before quenching in isopentane cooled in liquid nitrogen, to preserve sulfur speciation as close as possible to the *in vivo* condition, and to minimise chemical-fixation induced artefacts, as previously described.^{28, 32, 38} Samples were stored at 80°C until analysis.

HPLC analysis of plasma taurine

Taurine content of plasma was measured using reverse phase high performance liquid chromatography (HPLC) as previously described.¹¹ In brief, plasma samples were precipitated by addition of 10 times by weight of 5% trichloroacetic acid (TCA). After centrifugation, supernatants were collected and stored at -80°C until analysis. Analytes were separated using HPLC with fluorescent detection, with pre-column derivatisation with o-

1
2
3 phthalaldehyde (OPA) and 2-mercaptoethanol (2ME). OPA reacts rapidly with amino acids
4 and sulfhydryl groups to yield intensely fluorescent derivatives, and 2ME, a reducing agent,
5 prevents the OPA reagent from oxidising. An internal standard, o-phospho-dl-serine,
6 dissolved in 5% TCA was added to a final concentration of 5 mM. Sodium borate was used
7 to adjust the pH to 9. Samples were placed in an autosampler, which was maintained at 4°C.
8 Samples were mixed on a sample loop with a derivatising solution containing 40 mM OPA
9 and 160 mM 2ME in 100 mM sodium borate, pH 12, for 30 seconds before injection onto the
10 column. Separation was achieved with a C18 column (5 µl, 4.6 x 150 mm, Phenomenex)
11 using a Dionex Ultimate 3000 HPLC system. Mobile phase A consisted of 50 mM potassium
12 phosphate buffer, methanol and tetrahydrofuran (94:3:3). Mobile phase B consisted of 90%
13 methanol, with a gradient increase in B from 0 to 25%. Fluorescence was set at 360 nm and
14 455 nm for excitation and emission respectively.
15
16
17
18
19
20
21
22
23
24

25 **Quantitative histology**

26
27 Quadriceps muscles were cut in transverse sections (8 µm) were cut through the mid-region
28 of each muscle on a Leica CM3050S cryostat and were stained with Haematoxylin and
29 Eosin (H&E). For morphological analysis, non-overlapping tiled images of transverse muscle
30 sections were acquired using a Leica DM RBE microscope, a personal computer, a Hitachi
31 HVC20M digital camera, Image Pro Plus 4.5.1 soft-ware and Vexta stage movement
32 software. Tiled images were taken at 10x magnification.
33
34
35
36

37 Muscle morphology was drawn manually by the researcher using Image Pro Plus 4.5.1
38 software. The area occupied by necrotic myofibres (myofibres with fragmented sarcoplasm
39 and/or areas of inflammatory cells) was measured as a percentage (area) of the whole
40 muscle section. Since myofibres that have undergone previous necrosis exhibit central
41 nucleation, the amount of intact (peripheral nucleated) myofibres was measured, as a
42 percentage (area) of the whole muscle section. All section analysis was done 'blind'.
43 Histological analysis was completed as per the TREAT-NMD recommended standard
44 protocol "Histological measurements of dystrophic muscle – [https://treat-nmd.org/wp-](https://treat-nmd.org/wp-content/uploads/2016/08/MDX-DMD_M.1.2.007-28.pdf)
45 content/uploads/2016/08/MDX-DMD_M.1.2.007-28.pdf.
46
47
48
49
50
51
52
53

54 **Inflammatory cell presence (MPO)**

55
56 Myeloperoxidase (MPO) is an enzyme secreted by inflammatory cells (primarily neutrophils)
57 and MPO activity is a useful biomarker of neutrophils in tissues.^{39, 40} The enzyme MPO
58 catalyses the production of hypochlorous acid from hydrogen peroxide and chloride,⁴¹ and
59
60

1
2
3 hypochlorous acid reacts with 2-[6-(4-aminophenoxy)-3-oxo-3H-xanthen-9-yl]benzoic acid
4 (APF) to form the highly fluorescent compound fluorescein, that is measured in this method,
5 as previously described.⁴² Briefly, frozen quadriceps muscle was ground using a mortar and
6 pestle under liquid nitrogen and homogenised in 0.5% hexadecyltrimethylammonium
7 bromide in phosphate buffered saline (PBS). Samples were centrifuged and supernatants
8 diluted in PBS. Human MPO was used as the standard for the assay (Cayman Chemical).
9 Aliquots of each experimental sample or MPO standard were pipetted into a 384 well plate,
10 before the addition of APF working solution (20 μ M APF and 20 μ M hydrogen peroxide in
11 PBS) was added. The plate was incubated at room temperature (protected from light) for 30
12 minutes, with the fluorescence being measured every minute using excitation at 485 nm and
13 emission at 515-530 nm. The rate of change of fluorescence for each sample was compared
14 to that of the standards and results were expressed per mg of protein, quantified using the
15 DC protein assay (Bio-Rad).
16
17
18
19
20
21
22
23

24 **Tissue processing for XANES analysis**

25
26 Tissue sections (20 μ m) were cut from flash-frozen tissue blocks at -18 °C, using a cryo-
27 microtome. Tissue sections were mounted onto sulfur free, and optically transparent plastic
28 coverslips (Thermanox®). The tissue sections were air-dried and stored in the dark with
29 desiccant until XANES analysis. All samples were analysed within 5 days of tissue
30 sectioning. Although Thermanox plastic coverslips are optically transparent, they provide
31 poorer quality histology when compared to glass microscope slides. Therefore, additional
32 serial muscle tissue sections (10- μ m-thick) were cut and mounted onto conventional glass
33 microscope slides for haematoxylin and eosin (H&E) microscopy.
34
35
36
37
38
39

40 **Histology and Light Microscopy**

41
42 Air-dried tissue sections mounted on glass microscope slides were post-fixed for 30 minutes
43 in 10% formalin in PBS, pH 7.4. Sections on Thermanox® plastic coverslips were fixed post
44 XANES analysis, using the fixation protocol described above. The tissue sections were then
45 subjected to H&E staining with haematoxylin and counter stained with eosin. Unless
46 otherwise stated, microscopy images of H&E stained tissue were collected at 4x
47 magnification (Sections on Thermanox®) and 4x and 20x magnification (sections mounted
48 on glass microscope slides) using a Olympus Bx51 microscope with Olympus dp70 camera
49 and cellSans Standard software.
50
51
52
53
54

55
56 Factors affecting quality of H&E histology – As these experiments required international
57 transport of tissue sections without fixation, the H&E histology obtained from tissue sections
58 prepared for synchrotron analysis shows substantial colour variation and is of poorer quality
59
60

1
2
3 than would typically be expected. We have previously reported and commented on this
4 effect, which appears unavoidable as chemical fixation can not be used prior to synchrotron
5 analyses.³⁵
6
7

8 **XANES Analysis**

9

10 *Standard Compounds for Fitting* – The sulfur K-edge XANES spectra of standard
11 compounds were acquired in a previous study,²⁸ and represent thiols (reduced glutathione),
12 thio-ethers (methionine), disulfides (oxidised glutathione), sulfoxides (methionine sulfoxide),
13 sulfenic acids (hypotaurine), sulfonic acids (taurine), O-linked sulfate esters (dextran sulfate),
14 N-linked sulfate esters and inorganic sulfates (Na₂SO₄) functional groups. The XANES
15 spectra for these compounds were acquired from 30 - 100 mM solutions in PBS at pH 7.4
16 (to minimise the self-absorption artifacts as previously reported).^{37, 43} The spectra for the
17 standard compounds were acquired at beamline 4-3 of the Stanford Synchrotron Radiation
18 Lightsource (SSRL), as described previously.²⁸
19
20
21
22
23
24

25 *XANES-imaging and Micro-XANES spectroscopy* – Sulfur K-edge XANES-imaging and
26 micro-XANES spectra data collected at beamline 14-3 at SSRL. The beamline details were
27 as previously described; a monochromatized incident beam was generated from a Si(111)
28 double crystal, and a micro-focussed spot produced through focussing the incident x-ray
29 beam through a Kirkpatrick-Baez (KB) mirror pair (spot size at some was ~ 5 μm × 7 μm).^{33,}
30
31
32
33
34
35
36
37
38
39
40
41
42
43
44
45
46
47
48
49
50
51
52
53
54
55
56
57
58
59
60
The beamline energy was calibrated using the spectrum of a Na₂S₂O₃.5H₂O powder solid
standard, with the lowest energy peak set to 2469.2 eV, as described previously.^{33, 35} A
helium filled ion chamber was used to measure the incident intensity of the x-ray beam
upstream of the KB optics. For analysis, the samples were mounted at 45° to the incident
beam, in a sample box purged with He. The fluorescence emission from the sample was
measured with a single element Vortex Si drift fluorescence detector, which was mounted at
90° to the incident beam. The detector readout was synchronised to the stage movement
speed, and data collected continuously, such that the full emission spectrum was collected
every 500 ms, for an average stage movement (pixel size) of 20 μm (i.e., “rapid” or “fly”
scanning), as previously described.^{33, 35}

The full emission spectrum was recorded at each pixel, in addition to single channels for P,
S, and Compton scatter. The XANES-imaging protocol to specifically image taurine (i.e.,
chemically specific imaging) used sulfur X-ray fluorescence images at incident energies of
2475, 2478.2, 2479.8 and 2510 eV, using the method previously described.^{33, 35} Full micro-
XANES spectra were collected from representative sample positions, within the tissue
regions imaged with XANES-imaging.

1
2
3 *X-ray Data Processing* – Micro-XANES spectra were processed using the EXAFSPAK
4 program suite, as described previously.^{28, 33, 35} The DATFIT program was used to fit micro-
5 XANES spectra collected from tissue sections to linear combinations of reference spectra.
6 Standards were excluded from the fits unless they contributed at least 0.5% of the total
7 spectra, at a value greater than three times their standard deviation of measurement
8 (calculated from the diagonal elements of the variance-covariance matrix), as described
9 previously.^{28, 33, 35} All spectra from muscle tissue could be fitted to a linear sum of thiol, thio-
10 ether, disulfide, sulfoxide, and sulfonic acid functional groups. Sulfinic acids, N-linked sulfate
11 esters, O-linked sulfate esters and inorganic ‘free’ sulfate were not detected, and excluded
12 from the fitting refinement.
13

14
15
16
17
18
19
20 Chemically specific images were generated using Sam’s Micro-Analysis Tool Kit
21 (<http://smak.sams-xrays.com/>),⁴⁴ and Image J JV1.36
22 (<http://rsb.info.nih.gov/ij/download.html>), using the previously published method.^{33, 35} In brief,
23 to visualize n chemical forms of sulfur, $n + 2$ fluorescence maps of sulfur are collected. A
24 map is collected with incident energy tuned to the energy of the strongest peak of each of
25 the n chemical forms of sulfur, plus two additional maps below and above the sulfur K-edge,
26 respectively equivalent to a background, non-sulfur fluorescence map and a total sulfur map.
27 To image taurine, maps were collected at 2478.2 eV (strongest peak of taurine) and 24798
28 eV (strongest peak of sulfate esters, which may have overlapped with taurine spectrum).
29 The background fluorescence map is subtracted from each of the remaining $n + 1$
30 fluorescence maps. The background image was recorded at 2475 eV for four energy
31 approach to specifically image taurine. Normalized fluorescence intensities were determined
32 from model compound spectra of the n sulfur chemical forms (Table S1). With each pixel
33 intensity expressed as a linear combination of the normalized intensity of components
34 multiplied by their abundance at that pixel, simultaneous equations are solved by matrix
35 inversion to yield maps for the n sulfur chemical forms. Dividing by the total sulfur map (2510
36 eV) expresses the sulfur in each chemical form as percentage of total sulfur.
37
38
39
40
41
42
43
44
45
46

47 The average taurine content was calculated for each sample from regions of interest drawn
48 around anatomical structure of the tissue using bright field microscope images of the
49 unstained tissue section (before XANES analysis) and H&E stained section post XANES
50 analysis.
51
52
53

54 55 56 **Statistics / data analysis**

57
58 Statistical analysis was used to determine differences in the thiol, thio-ether, disulfide,
59 sulfoxide, and sulfonic acid (taurine) content (measured from micro-XANES) of muscle
60

1
2
3 tissue between wildtype, mdx, and mdx + taurine experimental groups. Statistical analysis
4 was also used to determine differences in taurine content measured in the muscle tissue
5 using XANES-imaging, for the same experimental groups. For both sets of statistical
6 analysis a One-Way ANOVA was used, with significance set to the 95% confidence interval
7 ($p < 0.05$). If a significant effect was found, post-hoc multi-comparison testing was
8 performed, using a Tukey's post-hoc test, and the 95% confidence interval ($p < 0.05$).
9
10
11
12
13
14
15
16
17
18
19
20
21
22
23
24
25
26
27
28
29
30
31
32
33
34
35
36
37
38
39
40
41
42
43
44
45
46
47
48
49
50
51
52
53
54
55
56
57
58
59
60

RESULTS

Mdx mice display classical features of dystrophic pathology, which is partly attenuated with taurine treatment.

To ensure taurine treatment was successful at increasing taurine content of mdx mice, and to confirm this treatment led to a decrease in dystropathology as previously reported, plasma taurine content was measured, as was muscle morphology (by quantitative H&E, representative images shown in Figure 1A-F) and inflammatory neutrophil cell presence (by MPO activity).

There was no difference in plasma taurine content when comparing mdx and C57 mice (Fig. 1G), however taurine treatment of mdx mice (Tmdx) increased plasma taurine content ($p = 0.0045$, Fig. 1G). Myofibre necrosis was increased in mdx compared to C57 muscle ($p = 0.0057$, Fig. 1H), and taurine treatment of mdx mice did not decrease myofibre necrosis (Fig. 1H). The percentage of intact myofibres (myofibres that have not undergone prior necrosis) was increased in mdx compared to C57 muscle ($p < 0.0001$, Fig. 1I), and taurine treatment of mdx mice increased the percentage of intact myofibres, indicating a protection from prior necrosis ($p < 0.0001$, Fig. 1I). Evidence of prior necrosis can be observed through H&E histology (Figure 1A-F) via the presence of centrally nucleated myofibres. MPO activity was increased in mdx compared to C57 muscle ($p = 0.0028$, Fig. 1J), and taurine treatment of mdx mice decreased MPO activity in muscle ($p = 0.0458$, Fig. 1J).

XANES Spectroscopy at the Sulfur K-edge demonstrates that mdx pathology reduces muscle taurine content, while therapeutic taurine supplementation increases muscle taurine content.

XANES spectroscopy at the sulfur K-edge was used to investigate total taurine content *in situ*, within *ex vivo* muscle tissue sections. Micro-XANES spectra of muscle tissue revealed that multiple chemical forms of sulfur can be detected in muscle tissue (Fig. 2). The XANES spectra of model compounds representing the different classes of sulfur detected in the muscle tissue include thiols (e.g., cysteine), thio-ether (e.g., methionine), disulfides (e.g., methionine sulfoxide) and sulfonic acids (e.g., taurine) as presented in Fig. 2A. Fitting the model compounds to XANES spectra collected from myofibres of wildtype control, mdx, and Tmdx tissue (Fig. 2B shows representative example of XANES fitting), indicated that taurine levels are depleted within myofibres of mdx mice, and treatment of mdx mice with taurine supplementation (Tmdx) prevented or counteracted this depletion (Fig. 2C).

XANES spectroscopy enabled quantification of different chemical forms of sulfur (including taurine) as a percentage of total sulfur in the tissue (Fig. 3A-F). There was no difference in

1
2
3 thiol content when comparing mdx and C57 muscle (Fig. 3A), however taurine treatment of
4 mdx mice (Tmdx) decreased thiol content in muscle ($p = 0.0196$, Fig. 3A). There was no
5 difference in thio-ether content of muscle from any group (Fig. 3B). Disulfide content was
6 increased in mdx compared to C57 muscle ($p < 0.0029$, Fig. 3C) suggesting increased
7 oxidative stress, and taurine treatment of mdx mice decreased disulfide content in muscle (p
8 = 0.0002, Fig. 3C), suggesting a suppression of oxidative stress. There was no difference in
9 sulfoxide content of muscle from any group (Fig. 3D). Taurine content was decreased in mdx
10 compared to C57 muscle ($p = 0.011$, Fig. 3E), and taurine treatment of mdx mice increased
11 taurine content in muscle ($p = 0.0002$, Fig. 3E).
12
13

14
15
16
17
18 *Chemical specific XANES-imaging (CSI) reveals that taurine localisation is*
19 *associated with infiltrating immune cells in mdx muscle tissue, but taurine does not solely*
20 *associate with infiltrating immune cells in Tmdx muscle tissue.*
21
22

23 Chemically specific XANES-imaging (CSI) was used to directly determine relative taurine
24 content in muscle tissue, and associate relative taurine levels with histology of the same
25 tissue (Fig. 3F and 4). Similar to the findings with XANES spectroscopy at the sulfur K-edge,
26 taurine content was decreased in mdx compared to C57 muscle ($p = 0.0015$, Fig. 3F), and
27 taurine treatment of mdx mice increased taurine content in muscle relative to mdx mice ($p <$
28 0.0001, Fig. 3F). Additionally, taurine content was found to be greater in taurine treated mdx
29 muscle relative to C57 muscle ($p = 0.0081$, Fig. 3F).
30
31
32
33
34

35 Taurine distribution was homogenous in wildtype mice, and histology did not reveal evidence
36 of infiltrating immune cells (Fig. 4A-C). However, the taurine distribution was heterogenous
37 in mdx mice (Fig. 4F), and comparison of chemically specific XANES taurine images with
38 H&E histology indicted that locally elevated taurine colocalised with infiltrating immune cells
39 (Fig. 4D-F). In contrast, overlay of chemically specific XANES taurine images with H&E
40 histology indicated that regions of elevated taurine in Tmdx muscle did not colocalise with
41 immune cells, because histology did not show evidence of cell nuclei at the location of
42 prominent taurine hotspots (Fig. 4H-I).
43
44
45
46
47
48
49
50
51
52
53
54
55
56
57
58
59
60

DISCUSSION

In this study we have used XANES imaging, in combination with H&E histology, to investigate muscle taurine distribution in taurine treated mdx mice. The combination of XANES imaging with histology has enabled this study for the first time to associate taurine content with markers of oxidative stress (disulfides), necrotic myofibres, and with infiltrating immune cells. These results provide direct evidence that although infiltrating immune cells elevate muscle taurine content, taurine treatment gives rise to increased intracellular muscle taurine that is independent of taurine localised within immune cells.

Although the main focus of XANES analysis in this study was to reveal taurine distribution, the XANES analysis also enabled other chemical forms of sulfur, such as thiols and disulfides to be measured. As shown in Figures 2 and 3, disulfides were increased in mdx muscle, consistent with our previous studies that show increased oxidative stress, particularly protein thiol oxidation, in mdx muscle.⁷⁻¹² Taurine treatment of mdx mice led to a decrease in muscle disulfides, suggesting an amelioration of oxidative stress (as discussed below). Additionally, taurine treatment of mdx mice lead to decrease in total thiols in the muscle, suggesting an amelioration of sulfur amino acid dysfunction, as we have previously reported in mdx mice.²⁴

Taurine is considered essential for the function of skeletal muscle, where it functions in the control of ion channel function, membrane stability and calcium homeostasis.¹³⁻¹⁷ Taurine levels have previously been shown to be decreased in mdx muscles before and during the onset of dystropathology (between three and six weeks); this deficiency diminishes as the disease pathology stabilises in adult mice.^{24, 29, 45} In the current study, we present new data obtained from direct *in situ* chemical measurement that this deficiency is a result of a decrease in taurine content of the myofibres, rather than a paucity of taurine in the extracellular space or other cells presence in the muscle (such as immune cells). However, as sub-cellular resolution was not possible in this study, we cannot rule out that taurine depletion, is also occurring in the extracellular space.

The exact cause of the taurine deficiency in mdx muscle is unknown, however since we show no differences in taurine content of mdx and C57 plasma, it is likely due to modulations in taurine uptake into myofibres. The maintenance of the intracellular taurine pool depends on active uptake from the extracellular space by the high affinity, low capacity, Na⁺ dependent transporter, TauT,⁴⁶ and we have previously shown mdx muscle to be deficient in this protein.²⁴ In the current study, we also show that taurine treatment of mdx mice leads to an increase in uptake of taurine by myofibres; this is a new observation as previous studies have not had the capability to differentiate myofibre taurine from 'whole muscle' taurine,

1
2
3 which includes taurine in the extracellular space, and other cells that are present (including
4 the taurine rich neutrophils).
5

6
7 This increase in myofibre taurine by taurine treatment of mdx mice was accompanied by
8 protection of myofibres from damage (shown by an increase in the percentage of intact
9 myofibres), and a decrease in muscle neutrophil presence. While taurine has many functions
10 *in vivo*, we hypothesise that it protects dystrophic muscle by its ability to act as an
11 antioxidant, since taurine can directly scavenge tissue oxidants. Neutrophils produce a
12 highly reactive oxidant called hypochlorous acid (HOCl), that targets proteins by reacting
13 with thiols and by causing oxidative damage.^{47, 48} HOCl is scavenged by taurine by the
14 formation of taurine chloramines that are much less reactive than HOCl, and also exerts anti-
15 inflammatory effects.⁴⁹⁻⁵¹ Therefore we also hypothesised that exogenous taurine is
16 protective of dystrophic muscle by the increased uptake of taurine by neutrophils, leading to
17 a decrease in HOCl content in muscle. However, our current data suggest that taurine
18 treatment may exert therapeutic benefit by directly increasing taurine content of myofibres.
19 Nonetheless, taurine may still be protecting dystrophic muscle by scavenging HOCl, since
20 HOCl secreted by neutrophils can cross membranes and diffuse across tissue.⁵² The
21 hypothesis that taurine is protecting dystrophic via scavenging of HOCl is supported by the
22 observation that taurine ameliorates the increased percentage of disulfide sulfurs observed
23 in mdx muscle. Thiol side chains of sulfur containing species (such as glutathione and
24 cysteine) are highly susceptible to extremely rapid reactions with HOCl, resulting in the
25 formation of disulfides.⁴⁸ Further experimental work is required however to better understand
26 the mechanism by which taurine protects dystrophic muscle, such as increasing spatial
27 resolution of the method to elucidate changes in taurine at the sub-cellular level.
28
29
30
31
32
33
34
35
36
37
38
39
40
41
42

43 **CONCLUSIONS & FUTURE WORK**

44
45 We and others have shown that taurine treatment of mdx mice leads to a decrease in
46 myofibre necrosis, an improvement in both *in vivo* and *ex vivo* muscle strength, increased
47 fatigue resistance and decreased inflammation and oxidative stress.^{8, 9, 11, 19-23} This protective
48 effect of taurine was presumed to be due to increased myofibre content of taurine levels, but
49 prior to this study there was no direct evidence of this. As immune cells such as neutrophils
50 are rich in taurine, and taurine is also found in the extracellular space and in plasma,
51 commonly used biochemical assays of muscle taurine cannot accurately quantify myofibre
52 taurine. Using direct spectroscopic imaging in this study we have been able to directly show
53 that taurine is depleted from mdx myofibres, and taurine supplementation ameliorates this
54 deficiency. Furthermore, we observed that areas of high taurine in taurine treated mdx
55
56
57
58
59
60

1
2
3 muscle did not co-localise with immune cell infiltration, suggesting that it is unlikely that
4 taurine uptake by neutrophils is the mechanism by which taurine protects mdx muscle.
5

6
7 Our study was limited by the spatial resolution available with the current X-ray optics (~10 -
8 20 μm) to perform chemical specific imaging XANES measurements at the sulfur K-edge.
9
10 This spatial resolution was not sufficient to resolve individual cells, or sub-cellular organelles.
11
12 Further, although X-ray imaging is often viewed as 'non-destructive', the quality of H&E from
13 tissue sections subjected to X-ray analysis was poor relative to what can be achieved from
14 flash frozen tissue sections, which limits the level of anatomical detail that can be inferred.
15
16 However, future developments in this field are likely to make direct taurine imaging possible
17 at the cellular and sub-cellular level. Such developments will enable future studies to further
18 investigate mechanisms through which changes in taurine content of mdx muscle affect
19 dystrophia.
20
21
22
23
24

25 **Conflicts of interest**

26
27 There are no conflicts to declare.
28
29
30

31 **Acknowledgements**

32
33 Components of this research were funded by the French Muscular Dystrophy Association
34 (AFM), and is gratefully acknowledged by JRT and PGA. Use of the Stanford Synchrotron
35 Radiation Lightsource, SLAC National Accelerator Laboratory, is supported by the U.S.
36 Department of Energy, Office of Science, Office of Basic Energy Sciences under Contract
37 No. DE-AC02-76SF00515. The SSRL Structural Molecular Biology Program is supported by
38 the DOE Office of Biological and Environmental Research, and by the National Institutes of
39 Health, National Institute of General Medical Sciences (P41GM103393). The contents of
40 this publication are solely the responsibility of the authors and do not necessarily represent
41 the official views of NIGMS or NIH. We gratefully acknowledge travel funding from the
42 Australian Synchrotron – international synchrotron access program, provided by ANSTO,
43 funded by the Australian Government.
44
45
46
47
48
49
50
51
52
53
54

55 **REFERENCES**

- 56
57
58 1. K. Bushby, R. Finkel, D. J. Birnkrant, L. E. Case, P. R. Clemens, L. Cripe, A. Kaul, K.
59 Kinnett, C. McDonald, S. Pandya, J. Poysky, F. Shapiro, J. Tomezsko, C. Constantin
60 and D. M. D. C. C. W. Group, *Lancet Neurol.*, 2010, **9**, 77-93.

2. M. D. Grounds, *Cell. Mol. Life Sci.*, 2008, **65**, 1621-1625.
3. W. D. Biggar, *Pediatr. Rev.*, 2006, **27**, 83-88.
4. G. Bulfield, W. Siller, P. Wight and K. Moore, *Proc. Natl. Acad. Sci. U. S. A.*, 1984, **81**, 1189-1192.
5. J. K. McGeachie, M. D. Grounds, T. A. Partridge and J. E. Morgan, *J. Neurol. Sci.*, 1993, **119**, 169-179.
6. M. D. Grounds and J. Torrisi, *FASEB J.*, 2004, **18**, 676-682.
7. J. R. Terrill, A. Boyatzis, M. D. Grounds and P. G. Arthur, *Int. J. Biochem. Cell Biol.*, 2013, **45**, 2097-2108.
8. J. R. Terrill, G. J. Pinniger, J. A. Graves, M. D. Grounds and P. G. Arthur, *J. Physiol.*, 2016, **594**, 3095-3110.
9. J. R. Terrill, G. J. Pinniger, K. V. Nair, M. D. Grounds and P. G. Arthur, *PLoS ONE*, 2017, **12**, e0187317.
10. J. R. Terrill, H. G. Radley-Crabb, M. D. Grounds and P. G. Arthur, *Neuromuscul. Disord.*, 2012, **22**, 427-434.
11. J. R. P. Terrill, M. D. Grounds and P. G. Arthur, *PLoS Curr*, 2016, **8**.
12. G. J. Pinniger, J. R. Terrill, E. B. Assan, M. D. Grounds and P. G. Arthur, *J. Physiol.*, 2017, **595**, 7093-7107.
13. A. J. Bakker and H. M. Berg, *J. Physiol.*, 2004, **538**, 185-194.
14. E. J. Hamilton, H. M. Berg, C. J. Easton and A. J. Bakker, *Amino Acids*, 2006, **31**, 273-278.
15. R. J. Huxtable, *Physiol. Rev.*, 1992, **72**, 101-163.
16. U. Warskulat, U. Flogel, C. Jacoby, H. G. Hartwig, M. Thewissen, M. W. Merx, A. Molojavyi, B. Heller-Stilb, J. Schrader and D. Haussinger, *FASEB J.*, 2004, **18**, 577-579.
17. U. Warskulat, B. Heller-Stilb, E. Oermann, K. Zilles, H. Haas, F. Lang and D. Haussinger, *Methods Enzymol.*, 2007, **428**, 439-458.
18. D. C. Camerino, D. Tricarico, S. Pierno, J. F. Desaphy, A. Liantonio, M. Pusch, R. Burdi, C. Camerino, B. Fraysse and A. De Luca, *Neurochem. Res.*, 2004, **29**, 135-142.
19. A. De Luca, S. Pierno, A. Liantonio, M. Cetrone, C. Camerino, S. Simonetti, F. Papadia and D. C. Camerino, *Br. J. Pharmacol.*, 2001, **132**, 1047-1054.
20. A. De Luca, S. Pierno, A. Liantonio, M. Cetrone, C. Camerino, B. Fraysse, M. Mirabella, S. Servidei, U. T. Ruegg and D. Conte Camerino, *J. Pharmacol. Exp. Ther.*, 2003, **304**, 453-463.
21. A. Cozzoli, J. F. Rolland, R. F. Capogrosso, V. T. Sblendorio, V. Longo, S. Simonetti, B. Nico and A. De Luca, *Neuropathol. Appl. Neurobiol.*, 2011, **37**, 243-256.
22. R. F. Capogrosso, A. Cozzoli, P. Mantuano, G. M. Camerino, A. M. Massari, V. T. Sblendorio, M. De Bellis, R. Tamma, A. Giustino, B. Nico, M. Montagnani and A. De Luca, *Pharmacol. Res.*, 2016, **106**, 101-113.
23. D. M. Horvath, R. M. Murphy, J. P. Mollica, A. Hayes and C. A. Goodman, *Amino Acids*, 2016, DOI: 10.1007/s00726-016-2292-2, 1-11.
24. J. R. Terrill, M. D. Grounds and P. G. Arthur, *Int. J. Biochem. Cell Biol.*, 2015, **66**, 141-148.
25. S. W. Schaffer, C. J. Jong, K. Ramila and J. Azuma, *J. Biomed. Sci.*, 2010, **17**, S2.
26. G. B. Schuller-Levis and E. Park, *FEMS Microbiol. Lett.*, 2003, **226**, 195-202.
27. S. Madsen, O. P. Ottersen and J. Storm-Mathisen, *Neurosci. Lett.*, 1985, **60**, 255-260.
28. M. J. Hackett, S. E. Smith, P. G. Paterson, H. Nichol, I. J. Pickering and G. N. George, *ACS chemical neuroscience*, 2012, **3**, 178-185.
29. J. Griffin, H. Williams, E. Sang, K. Clarke, C. Rae and J. Nicholson, *Anal. Biochem.*, 2001, **293**, 16-21.
30. H. Bongers, F. Schick, M. Skalej, W.-I. Jung and A. Stevens, *Magn. Reson. Imaging*, 1992, **10**, 957-964.

- 1
 - 2
 - 3
 - 4
 - 5
 - 6
 - 7
 - 8
 - 9
 - 10
 - 11
 - 12
 - 13
 - 14
 - 15
 - 16
 - 17
 - 18
 - 19
 - 20
 - 21
 - 22
 - 23
 - 24
 - 25
 - 26
 - 27
 - 28
 - 29
 - 30
 - 31
 - 32
 - 33
 - 34
 - 35
 - 36
 - 37
 - 38
 - 39
 - 40
 - 41
 - 42
 - 43
 - 44
 - 45
 - 46
 - 47
 - 48
 - 49
 - 50
 - 51
 - 52
 - 53
 - 54
 - 55
 - 56
 - 57
 - 58
 - 59
 - 60
31. I. J. Pickering, E. Y. Sneeden, R. C. Prince, E. Block, H. H. Harris, G. Hirsch and G. N. George, *Biochemistry (Mosc.)*, 2009, **48**, 6846-6853.
32. M. J. Hackett, C. J. Britz, P. G. Paterson, H. Nichol, I. J. Pickering and G. N. George, *ACS chemical neuroscience*, 2015, **6**, 226-238.
33. M. J. Hackett, P. G. Paterson, I. J. Pickering and G. N. George, *Anal. Chem.*, 2016, **88**, 10916-10924.
34. M. Gnida, E. Yu Sneeden, J. C. Whitin, R. C. Prince, I. J. Pickering, M. Korbas and G. N. George, *Biochemistry (Mosc.)*, 2007, **46**, 14735-14741.
35. M. J. Hackett, G. N. George, I. J. Pickering and B. F. Eames, *Biochemistry (Mosc.)*, 2016, **55**, 2441-2451.
36. M. J. Hackett, S. E. Smith, S. Caine, H. Nichol, G. N. George, I. J. Pickering and P. G. Paterson, *Free Radical Biol. Med.*, 2015, **89**, 806-818.
37. I. J. Pickering, R. C. Prince, T. Divers and G. N. George, *FEBS Lett.*, 1998, **441**, 11-14.
38. M. J. Hackett, J. A. McQuillan, F. El-Assaad, J. B. Aitken, A. Levina, D. D. Cohen, R. Siegele, E. A. Carter, G. E. Grau and N. H. Hunt, *Analyst*, 2011, **136**, 2941-2952.
39. K. Setsukinai, Y. Urano, K. Kakinuma, H. J. Majima and T. Nagano, *J. Biol. Chem.*, 2003, **278**, 3170-3175.
40. C. C. Winterbourn, M. C. M. Vissers and A. J. Kettle, *Curr. Opin. Hematol.*, 2000, **7**, 53-58.
41. C. C. Winterbourn and A. J. Kettle, *Free Radic. Biol. Med.*, 2000, **29**, 403-409.
42. J. R. Terrill, M. N. Duong, R. Turner, C. Le Guiner, A. Boyatzis, A. J. Kettle, M. D. Grounds and P. G. Arthur, *Redox Biol*, 2016, **9**, 276-286.
43. I. J. Pickering, G. N. George, E. Y. Yu, D. C. Brune, C. Tuschak, J. Overmann, J. T. Beatty and R. C. Prince, *Biochemistry*, 2001, **40**, 8138-8145.
44. S. M. Webb, 2011.
45. L. McIntosh, K. E. Granberg, K. M. Brière and J. E. Anderson, *NMR Biomed.*, 1998, **11**, 1-10.
46. T. Ito, S. Oishi, M. Takai, Y. Kimura, Y. Uozumi, Y. Fujio, S. W. Schaffer and J. Azuma, *J. Biomed. Sci.*, 2010, **17**, 1-5.
47. C. C. Winterbourn, *Toxicology*, 2002, **181-182**, 223-227.
48. C. Storkey, M. J. Davies and D. I. Pattison, *Free Radic. Biol. Med.*, 2014, **73**, 60-66.
49. J. Marcinkiewicz and E. Kontny, *Amino Acids*, 2014, **46**, 7-20.
50. G. B. Schuller-Levis and E. Park, *Neurochem. Res.*, 2004, **29**, 117-126.
51. A. V. Peskin and C. C. Winterbourn, *Free Radic. Biol. Med.*, 2006, **40**, 45-53.
52. B. Halliwell and Gutteridge, *Free Radicals in Biology and Medicine*, Oxford University Press, NY, 2007.

1
2
3 **Fig. 1.** Characterisation of dystrophy in mdx. **(A,D)** H&E images of C57 quadriceps muscle
4 in cross section, with intact myofibres (peripheral nuclei, white arrow). **(B,E)** shows untreated
5 mdx quadriceps, with myofibres with fragmented sarcoplasm and areas of inflammatory cells
6 (black arrow) as well as large amounts of myofibres with central nuclei (indicating myofibres
7 that have previously undergone necrosis, white arrow). **(C,F)** shows taurine treated mdx
8 quadriceps muscle, with myofibres with fragmented sarcoplasm and areas of inflammatory
9 cells (black arrow) as well as an increase in myofibres with peripheral nuclei (indicating intact
10 myofibres that have not previously undergone necrosis, white arrow). Immune cells were not
11 observed outside of vasculature in wildtype controls (black arrow in panel D). **(G)** Bulk
12 taurine assay in blood plasma. **(H)** Assessment of muscle necrosis. **(I)** Quantification of
13 intact healthy muscle fibres. **(J)** Muscle immune cell (neutrophil) infiltration, as measured by
14 MPO activity.

15
16
17
18
19
20
21
22
23 One-way ANOVA and post-hoc testing was used to identify statistically significant
24 differences between means ($n = 5$ animal replicates in each group). * $p < 0.05$, ** $p < 0.01$,
25 *** $p < 0.001$.

26
27
28 Image regions D, E, F are shown by black dashed boarder on larger area image in panels A,
29 B, C.

30
31
32
33
34 **Fig. 2.** XANES sulfur K-edge analysis of muscle tissue from wildtype and mdx mice. **(A)**
35 XANES sulfur K-edge spectra of model compounds of different classes of sulfur compounds
36 (in order of increasing oxidation state from top to bottom). **(B)** Representative example of
37 fitting a XANES sulfur K-edge spectrum of muscle tissue to a linear sum of model compound
38 spectra. Raw data is shown as white circles with fit shown as solid line passing through. The
39 model compound spectra contributing to the fit are shown as solid black lines scaled to their
40 relative % contribution to the fit. The fit residual is shown underneath the spectra. **(C)**
41 Representative XANES sulfur K-edge spectra of from wildtype control, mdx, and Tmdx
42 muscle tissue. The black arrow at ~ 2478 eV indicates the location of taurine in the spectra,
43 highlighting the decreased taurine content observed in muscle tissue during mdx, and that
44 taurine supplementation (Tmdx) increases muscle taurine content. The black arrow at
45 ~ 2469.5 eV indicates the increased disulfide content, a marker of oxidative stress that is
46 observed in the mdx muscle tissue.

1
2
3
4
5
6
7
8 **Fig. 3.** XANES spectroscopy quantification of the different chemical forms of classes of sulfur in muscle tissue in wildtype and mdx muscle: (A) thiols, (B) thio-ether, (C) disulfides, (D) sulfoxides, (E) sulfonic acids (taurine). (F) Quantification of taurine in muscle tissue using XANES chemically specific imaging (CSI). One-way ANOVA and post-hoc testing was used to identify statistically significant differences between means ($n = 5$ animal replicates in each group). * $p < 0.05$, ** $p < 0.01$, *** $p < 0.001$.

9
10
11
12
13
14
15
16
17
18
19
20 **Fig. 4.** Chemically specific XANES imaging (CSI) of taurine and overlay with H&E histology of the same or adjacent tissue section in wildtype and mdx muscle. 4x magnification images were collected from the same tissue section as analysed with XANES imaging for mdx and wildtype tissues, and 20x magnification image was collected from the adjacent image. Both 4x and 20x were collected from the same tissue section as analysed with XANES imaging for Tmdx tissue. In general the H&E histology is poorer quality than normally achieved, due to the sample preparation, as described in the methods. (A-C) Representative muscle tissue from wildtype controls showing (A) overview H&E histology, (B) higher magnification histology view of a specific region of interest defined by the black box (in panel A), and (C) the overlay of CSI taurine image with the H&E histology. The overlay reveals relatively uniform taurine distribution, and the slight elevation of taurine at the location marked with the black arrow (in panel C) is colocalised with intravascular immune cells. (D-F) Representative muscle tissue from mdx mice showing (D) overview H&E histology, (E) higher magnification histology view of a specific regions of interest defined by the black box *i* and *ii* (in panel D), and (F) the overlay of CSI taurine image with the H&E histology. The overlay reveals an overall depletion of taurine in mdx mice relative to wildtype controls, however the taurine distribution is heterogenous in mdx muscles. Locally elevated regions of taurine in mdx tissue colocalised with immune cells within the muscle tissue (regions of interest *i* and *ii*), as shown at the location marked with the black arrows (in panel F). (G-I) Representative muscle tissue from Tmdx showing (G) overview H&E histology, (H) higher magnification histology view of a specific region of interest defined by the black box (in panel G), and (I) the overlay of CSI taurine image with the H&E histology. The overlay reveals that taurine is elevated in Tmdx tissue relative to wildtype controls and mdx mice. Further, regions of interest showing the highest taurine content in Tmdx tissue (black box in panel G and black arrow in panel I) did not colocalise with histological evidence of immune cells.

21
22
23
24
25
26
27
28
29
30
31
32
33
34
35
36
37
38
39
40
41
42
43
44
45
46
47
48
49
50
51
52
53
54
55
56
57
58
59
60

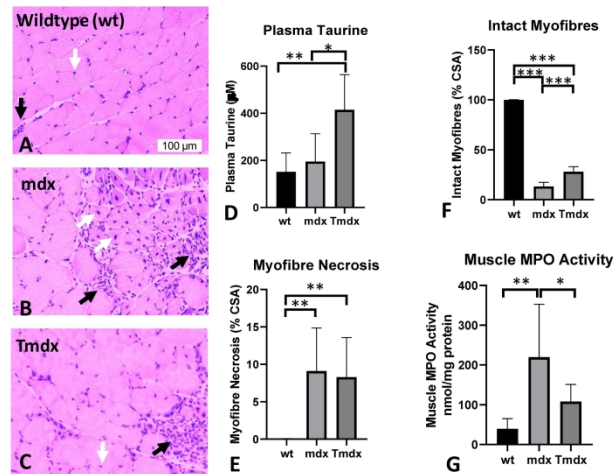


Fig. 1. Characterisation of dystrophy in mdx. (A,D) H&E images of C57 quadriceps muscle in cross section, with intact myofibres (peripheral nuclei, white arrow). (B,E) shows untreated mdx quadriceps, with myofibres with fragmented sarcoplasm and areas of inflammatory cells (black arrow) as well as large amounts of myofibres with central nuclei (indicating myofibres that have previously undergone necrosis, white arrow). (C,F) shows taurine treated mdx quadriceps muscle, with myofibres with fragmented sarcoplasm and areas of inflammatory cells (black arrow) as well as an increase in myofibres with peripheral nuclei (indicating intact myofibres that have not previously undergone necrosis, white arrow). Immune cells were not observed outside of vasculature in wildtype controls (black arrow in panel D). (G) Bulk taurine assay in blood plasma. (H) Assessment of muscle necrosis. (I) Quantification of intact healthy muscle fibres. (J) Muscle immune cell (neutrophil) infiltration, as measured by MPO activity.

One-way ANOVA and post-hoc testing was used to identify statistically significant differences between means (n = 5 animal replicates in each group). * p < 0.05, ** p < 0.01, *** p < 0.001.

Image regions D, E, F are shown by black dashed border on larger area image in panels A, B, C.

338x190mm (300 x 300 DPI)

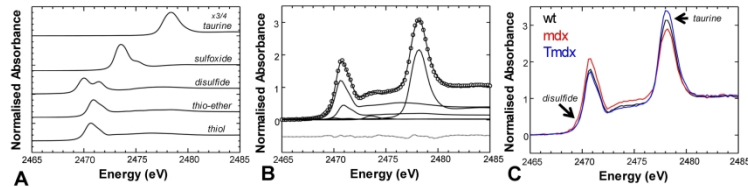


Fig. 2. XANES sulfur K-edge analysis of muscle tissue from wildtype and mdx mice. (A) XANES sulfur K-edge spectra of model compounds of different classes of sulfur compounds (in order of increasing oxidation state from top to bottom). (B) Representative example of fitting a XANES sulfur K-edge spectrum of muscle tissue to a linear sum of model compound spectra. Raw data is shown as white circles with fit shown as solid line passing through. The model compound spectra contributing to the fit are shown as solid black lines scaled to their relative % contribution to the fit. The fit residual is shown underneath the spectra. (C) Representative XANES sulfur K-edge spectra of from wildtype control, mdx, and Tmdx muscle tissue. The black arrow at ~ 2478 eV indicates the location of taurine in the spectra, highlighting the decreased taurine content observed in muscle tissue during mdx, and that taurine supplementation (Tmdx) increases muscle taurine content. The black arrow at ~ 2469.5 eV indicates the increased disulfide content, a marker of oxidative stress that is observed in the mdx muscle tissue.

338x190mm (300 x 300 DPI)

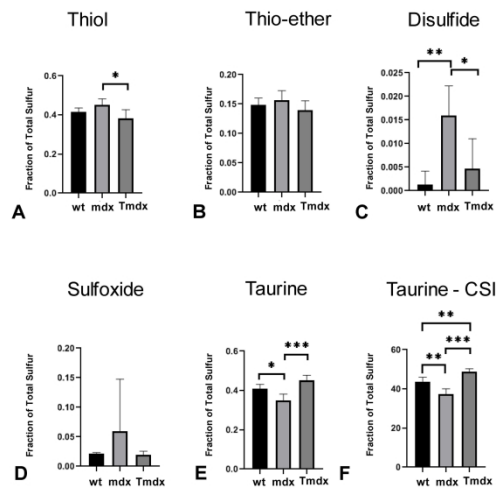


Fig. 3. XANES spectroscopy quantification of the different chemical forms of classes of sulfur in muscle tissue in wildtype and mdx muscle: (A) thiols, (B) thio-ether, (C) disulfides, (D) sulfoxides, (E) sulfonic acids (taurine). (F) Quantification of taurine in muscle tissue using XANES chemically specific imaging (CSI). One-way ANOVA and post-hoc testing was used to identify statistically significant differences between means ($n = 5$ animal replicates in each group). * $p < 0.05$, ** $p < 0.01$, *** $p < 0.001$.

338x190mm (300 x 300 DPI)

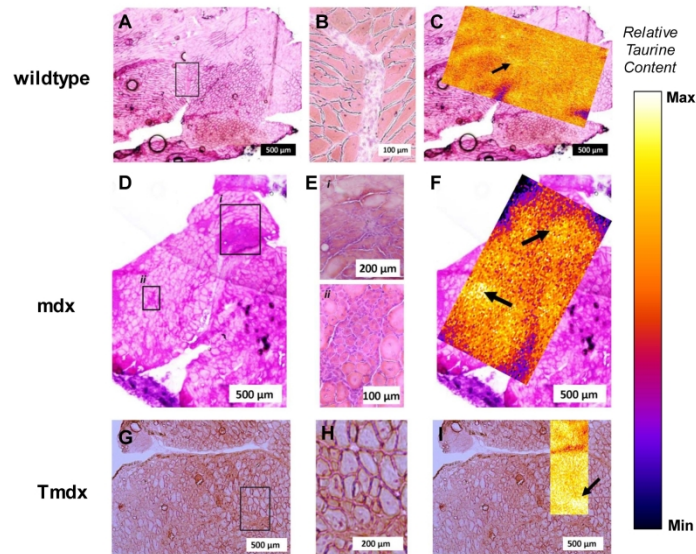
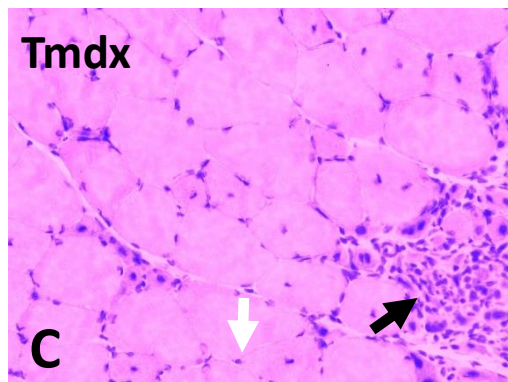
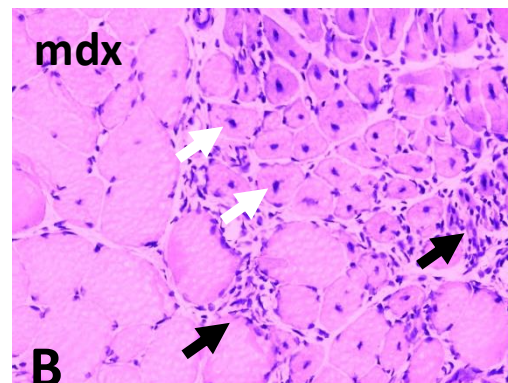
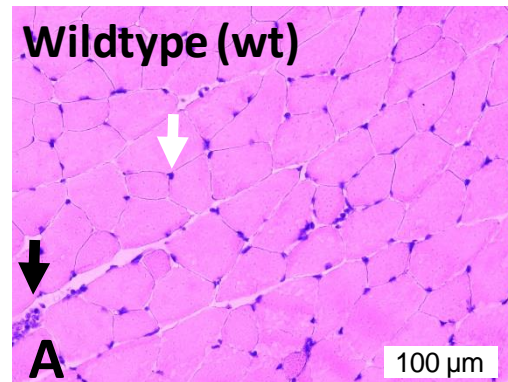


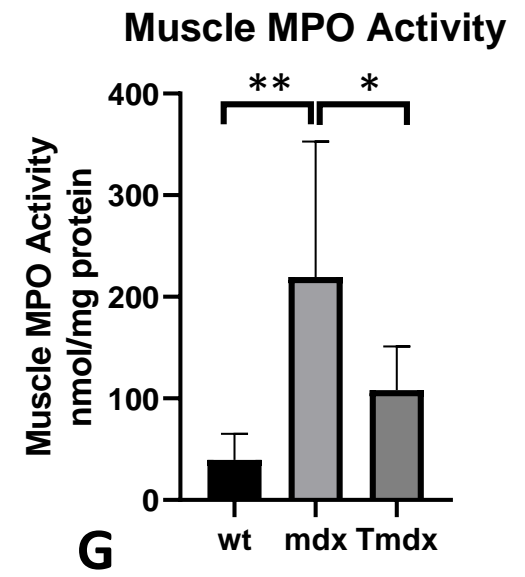
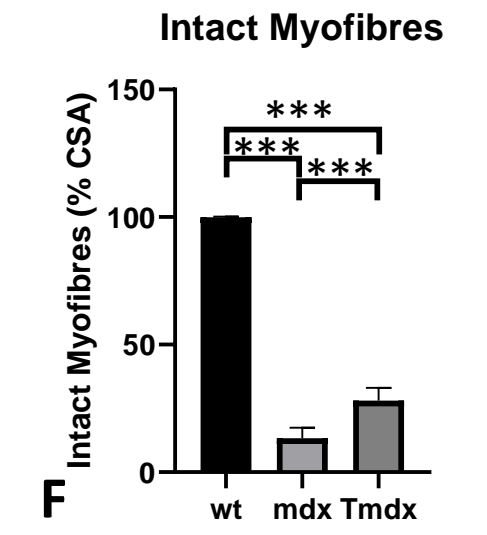
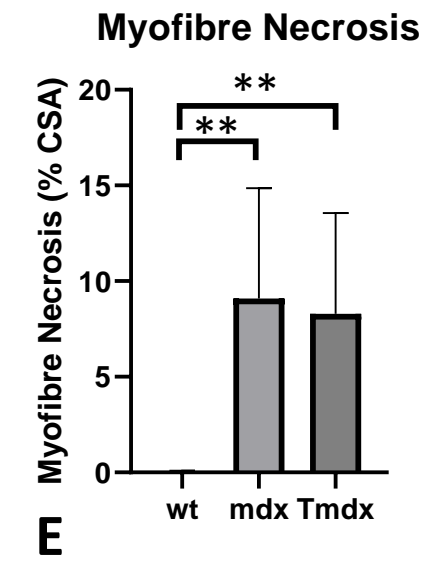
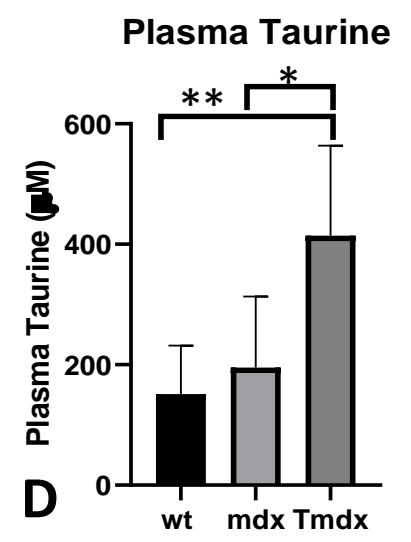
Fig. 4. Chemically specific XANES imaging (CSI) of taurine and overlay with H&E histology of the same or adjacent tissue section in wildtype and mdx muscle. 4x magnification images were collected from the same tissue section as analysed with XANES imaging for mdx and wildtype tissues, and 20x magnification image was collected from the adjacent image. Both 4x and 20x were collected from the same tissue section as analysed with XANES imaging for Tmdx tissue. In general the H&E histology is poorer quality than normally achieved, due to the sample preparation, as described in the methods. (A-C) Representative muscle tissue from wildtype controls showing (A) overview H&E histology, (B) higher magnification histology view of a specific region of interest defined by the black box (in panel A), and (C) the overlay of CSI taurine image with the H&E histology. The overlay reveals relatively uniform taurine distribution, and the slight elevation of taurine at the location marked with the black arrow (in panel C) is colocalised with intravascular immune cells. (D-F) Representative muscle tissue from mdx mice showing (D) overview H&E histology, (E) higher magnification histology view of a specific regions of interest defined by the black box i and ii (in panel D), and (F) the overlay of CSI taurine image with the H&E histology. The overlay reveals an overall depletion of taurine in mdx mice relative to wildtype controls, however the taurine distribution is heterogenous in mdx muscles. Locally elevated regions of taurine in mdx tissue colocalised with immune cells within the muscle tissue (regions of interest i and ii), as shown at the location marked with the black arrows (in panel F). (G-I) Representative muscle tissue from Tmdx showing (G) overview H&E histology, (H) higher magnification histology view of a specific region of interest defined by the black box (in panel G), and (I) the overlay of CSI taurine image with the H&E histology. The overlay reveals that taurine is elevated in Tmdx tissue relative to wildtype controls and mdx mice. Further, regions of interest showing the highest taurine content in Tmdx tissue (black box in panel G and black arrow in panel I) did not colocalise with histological evidence of immune cells.

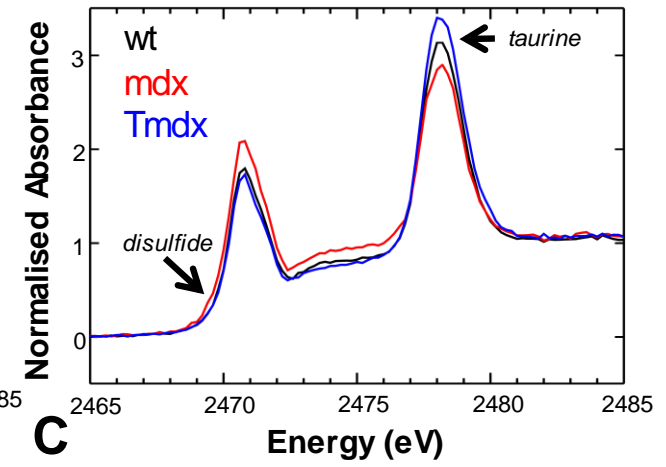
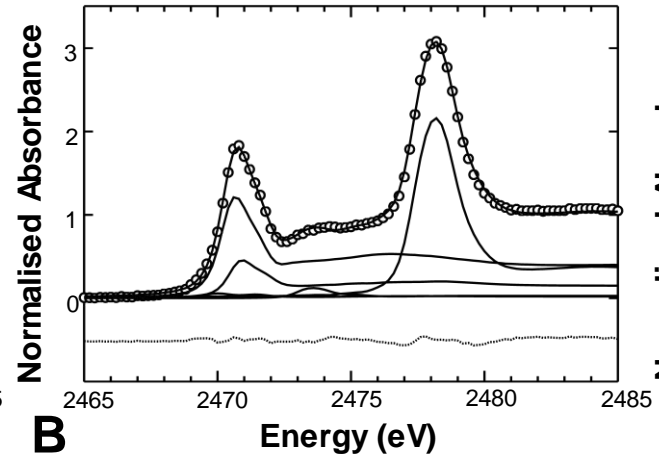
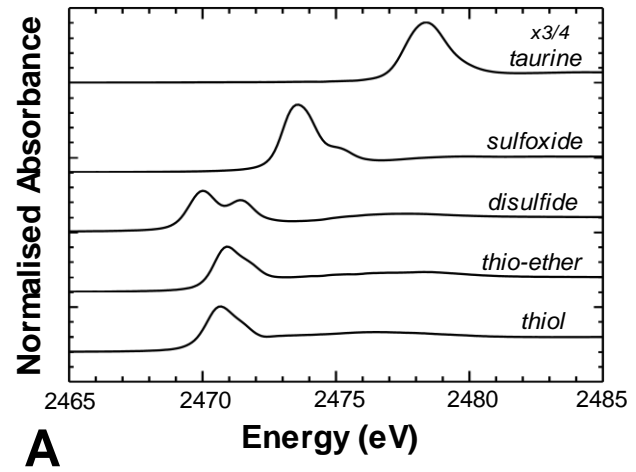
338x190mm (300 x 300 DPI)

1
2
3
4
5
6
7
8
9
10
11
12
13
14
15
16
17
18
19
20
21
22
23
24
25
26
27
28
29
30
31
32
33
34
35
36
37
38
39
40
41

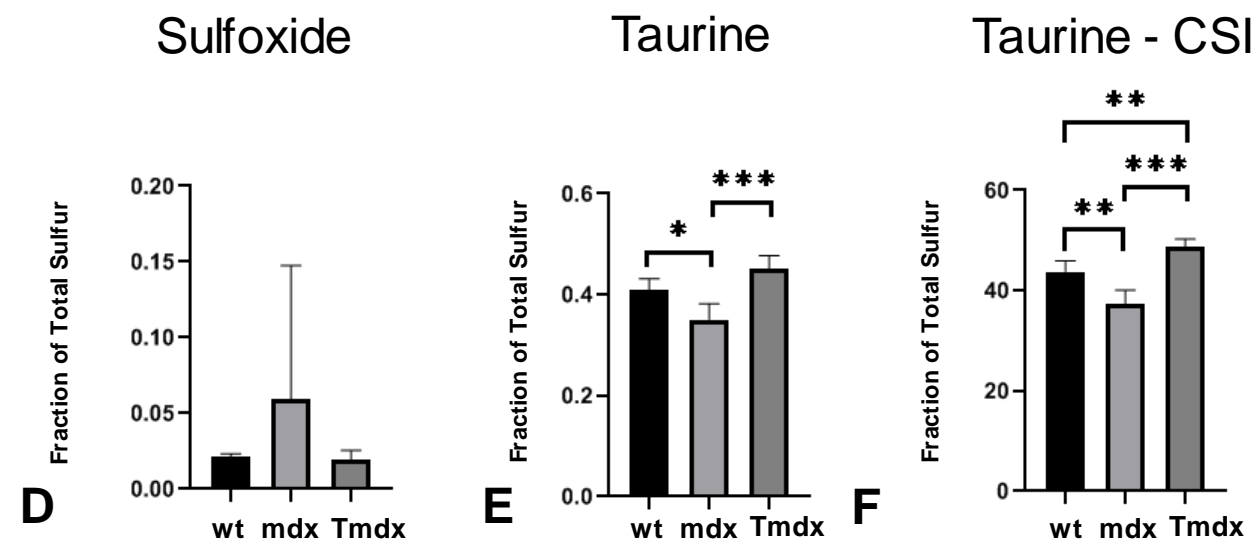
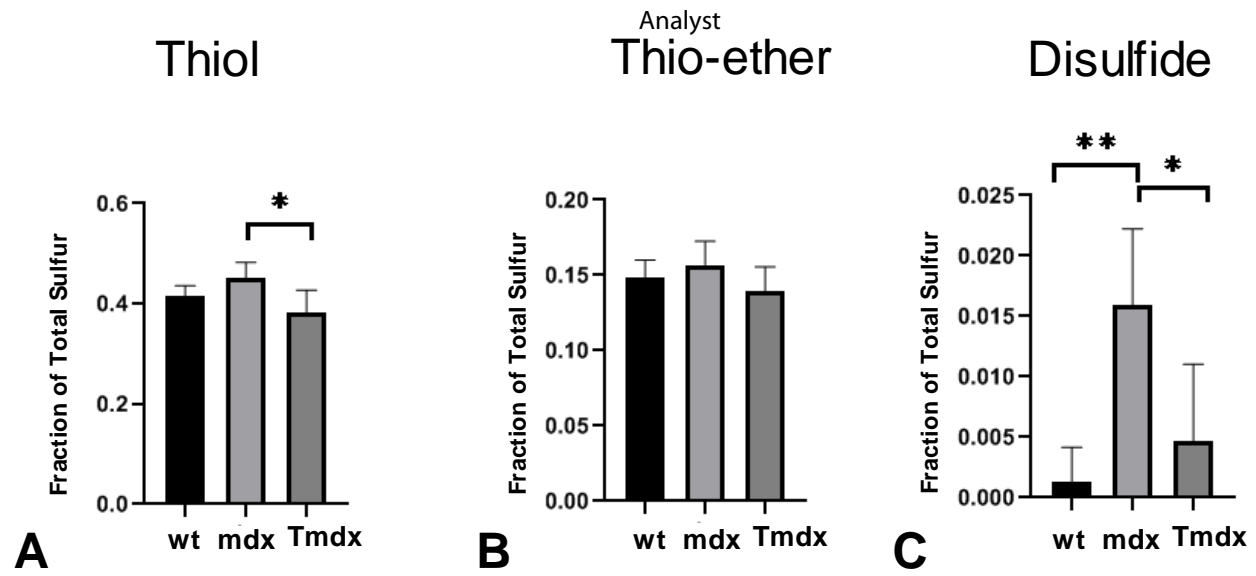


Analyst





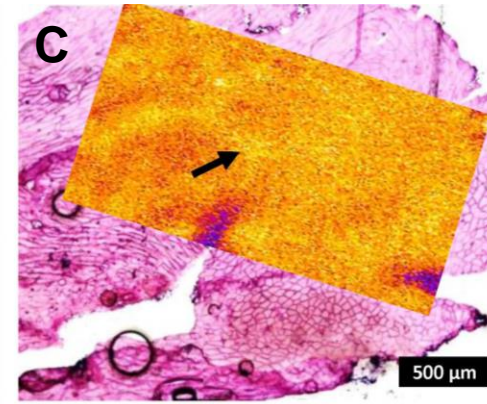
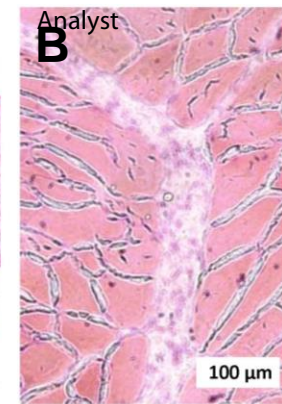
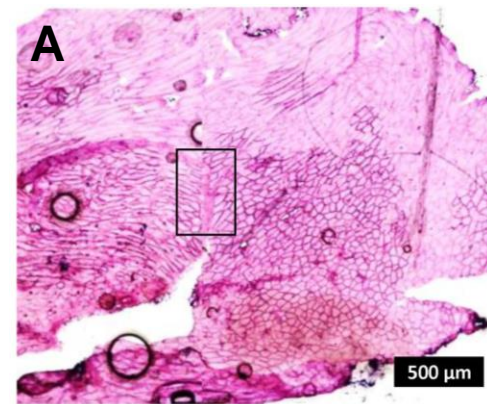
23
24
25
26
27
28
29
30
31
32
33
34
35
36
37
38
39
40
41



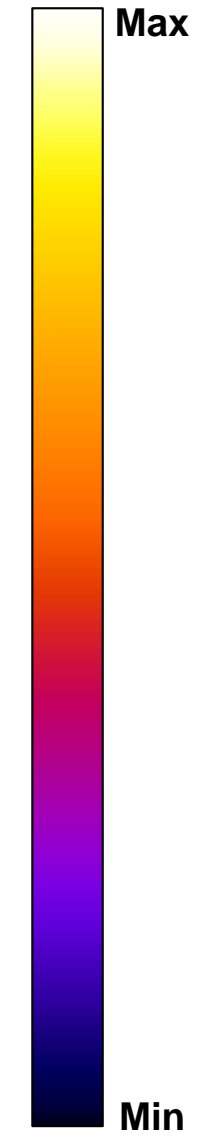
1
2
3
4
5
6
7
8
9
10
11
12
13
14
15
16
17
18
19
20
21
22
23
24
25
26
27
28
29
30
31
32
33
34
35
36
37
38
39
40
41

1
2
3
4
5
6
7
8
9
10
11
12
13
14
15
16
17
18
19
20
21
22
23
24
25
26
27
28
29
30
31
32
33
34
35
36
37
38
39
40
41

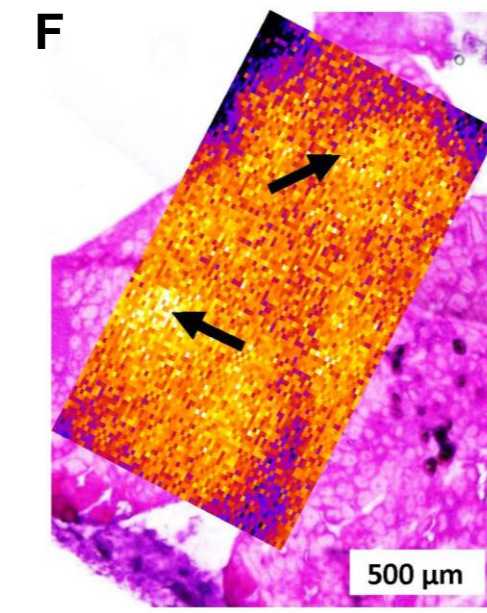
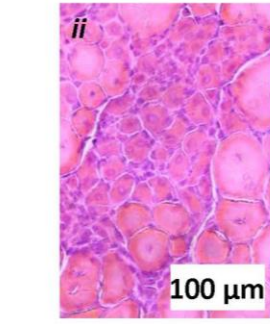
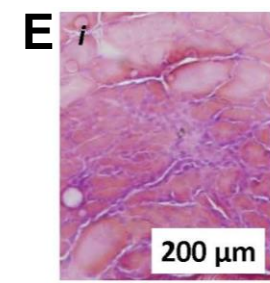
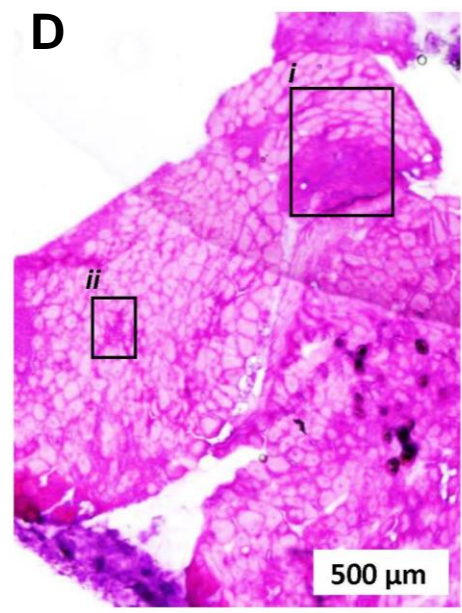
wildtype



Relative
Taurine
Content



mdx



Tmdx

